ELSEVIER

Journal of Structural Geology 27 (2005) 2159–2170

JOURNAL OF STRUCTURAL GEOLOGY

www.elsevier.com/locate/jsg

The development of subgrain misorientations with strain in dry synthetic NaCl measured using EBSD

G.M. Pennock*, M.R. Drury, C.J. Spiers

Faculty of Geosciences, Utrecht University, Postbus 80.021, 3508 TA Utrecht, The Netherlands

Received 7 February 2005; received in revised form 3 June 2005; accepted 29 June 2005
Available online 13 September 2005

Abstract

The development of subgrain boundary misorientations with strain in dry, synthetic NaCl polycrystals, deformed at elevated temperature, has been investigated using electron backscattered diffraction (EBSD). At low natural strains, up to 0.5, average misorientations of subgrain boundaries increase with strain and a power law relationship exists between strain and average misorientations. The average misorientations are strongly influenced by grain orientation, suggesting that the misorientation–strain relationship may also be texture dependent in materials with high plastic anisotropy, like NaCl. A slight grain size dependency of the average misorientations was observed. The results indicate that with suitable calibration, average subgrain boundary misorientations may offer a method for estimating the strain accommodated by dislocation creep in NaCl and thus perhaps in other geological materials, although current theories for polycrystalline plasticity imply that misorientations may also depend on stress in some situations.

Keywords: Dry NaCl; Subgrain; Misorientation; Strain; Grain size; EBSD

1. Introduction

The rheological behaviour of naturally deformed rocks is generally controlled by several different mechanisms that can operate simultaneously or consecutively and can affect the microstructure. Estimating strain from microstructures can therefore be difficult, especially when more than one deformation mechanism is operative (Passchier and Trouw, 1996). For instance, deformation at temperatures in the range 100–200 °C of synthetic NaCl, dried to contain only a few ppm of water, is dominated by dislocation creep and microstructures contain elongated grains and subgrains (Trimby et al., 2000; Watanabe and Peach, 2002; Ter Heege et al., 2005). When water is present, microstructures are dominated by grain boundary migration recrystallization (Spiers et al., 1986; Urai et al., 1986) but elongated grains, subgrains and free dislocations may still be present (Spiers and Carter, 1998). Although these microstructures show that dislocation creep has occurred, only small strains are needed to produce a high density of free dislocations, and subgrains form by 0.10 strain (Carter and Heard, 1970). This means that other less easily recognized processes, such as pressure solution creep (Spiers et al., 1990) or crack seal mechanisms may also have contributed to grain elongation processes and together with phenomena such as grain boundary sliding, may even be the major contributor to the bulk strain during deformation. The same argument applies equally to other rock types, such as quartz tectonites (Mitra, 1976; Harrison and Onasch, 2000).

As the presence of subgrains is sufficient only for establishing that dislocation activity has occurred, quantifying any systematic trends in subgrain development with strain in a given material may be useful for establishing a strain gauge for dislocation creep deformation, as well as providing insight into the role of subgrain rotation in dynamic recrystallization (Pennock et al., 2004). One potential method of assessing dislocation creep strain is to measure how the subgrain misorientation angle increases with strain. A small number of misorientations have been measured in various deformed materials using both light microscopy (LM) (Avé Lallement, 1985) and transmission

* Corresponding author. Tel.: +31 30 2535109; fax: +31 30 2537725.
E-mail address: gpennock@geo.uu.nl (G.M. Pennock).

0191-8141/$ - see front matter © 2005 Elsevier Ltd. All rights reserved.
doi:10.1016/j.jsg.2005.06.013

electron microscopy (TEM) (Hughes et al., 1997). More recently, many more subgrain misorientations have been measured with EBSD mapping in metals and NaCl (Randle and Engler, 2000; Humphreys, 2001; Pennock et al., 2002; Hurley and Humphreys, 2003; Pennock and Drury, 2005). The average misorientation of subgrain boundaries, θ_{av}, is frequently reported to show a power law relationship with strain, ε, of the form:

$$\theta_{av} \propto \varepsilon^{n} \quad (1)$$

where $n = 4$–6, depending on the type of subgrain boundary (Hughes et al., 1997; Pennock et al., 2002; Pennock and Drury, 2005).

Using EBSD, Pennock et al. (2002) and Pennock and Drury (2005) showed that individual subgrains in dry synthetic NaCl deformed in the dislocation creep regime were surrounded by segments of subgrain boundaries with a wide range of misorientations. Subgrain boundaries were separated into three types, depending on the boundary misorientation and spatial distribution. Equiaxed subgrain boundaries were ubiquitous, and generally had lower misorientations, whereas long straight subgrain boundaries had higher misorientations and extended between several subgrains: extended subgrains were often associated with either triple points or dissected grains. A weak core–mantle development of subgrains and subgrain boundaries was also noted. The formation of new grains by subgrain rotation recrystallization was limited in these materials at strains of 0.5 (Pennock et al., 2004).

Many variables, including strain, influence subgrain development and may influence misorientation values, such as deformation conditions (confining pressure, temperature and strain rate), material properties (grain orientation, neighbouring grain orientation, grain size and fluid content). The angular resolution of the technique used to measure misorientations (LM, TEM, EBSD) may also influence the range of misorientations that can be measured. Pennock et al. (2002) found that EBSD mapping variables, such as 'noise' caused by angular resolution limits, step size, processing of non-indexed pixels and filtering data to remove noise (Pennock and Drury, 2005), all influenced average misorientation values in NaCl, particularly using etched NaCl samples. However, the average misorientation parameter may still provide useful data on the state of a material, including the dislocation creep strain magnitude, depending on the scatter in the data produced by other effects and on whether the θ_{av} versus ε relationship is reproducible for all EBSD systems (Pennock and Drury, 2005). This paper examines the effect strain, grain orientation, texture and grain size have on the average misorientation values, with the aim of assessing the potential of θ_{av} versus ε relationships for estimating dislocation creep strain in geological materials.

2. Materials and methods

2.1. Sample preparation

Cylinders, 3 cm in diameter, were prepared from synthetic NaCl by cold pressing and annealing to a final density of ~99.5% (Peach and Spiers, 1996; Ter Heege, 2002). To minimize the occurrence of grain boundary migration recrystallization (Trimby et al., 2000) samples were dried in flowing argon, mostly to a water content of 5 ± 2 ppm (Watanabe and Peach, 2002) (Table 1). This procedure gave initial average grain sizes ranging from 300 to 400 μm, although variations in the drying sequence resulted in some variations in grain size between batches. The cylinders were deformed in axi-symmetric compression using a triaxial testing machine under a confining pressure of 50 MPa at 165 ± 10 °C (~0.4 Tm) and at constant displacement rate, equivalent to a final strain rate of $\sim 6 \times 10^{-7}$ s^{-1} (Peach and Spiers, 1996; Ter Heege, 2002; Ter Heege et al., 2005). Under these conditions dry NaCl does not undergo dynamic recrystallization by grain boundary migration and continues to work harden (Ter Heege et al., 2005). The samples deformed relatively homogeneously, although there was some minor barrelling at higher strains. Final natural strains ranged from 0.07 to 0.54 (Fig. 1). The 0.15 strain sample (PK119a) showed lower stress values, related to the slightly higher water content of this sample (11 ppm). Samples were cooled to room temperature (approximately 1.5 °C/min) and sectioned soon after deformation; sections were made of the central portion of the cylinder, parallel to the compression direction, and polished in a dry room (Urai et al., 1987). All sections were lightly etched for 10 s, either in saturated salt solution containing ferric chloride, or in methanol, and finally washed with either hexane or ether.

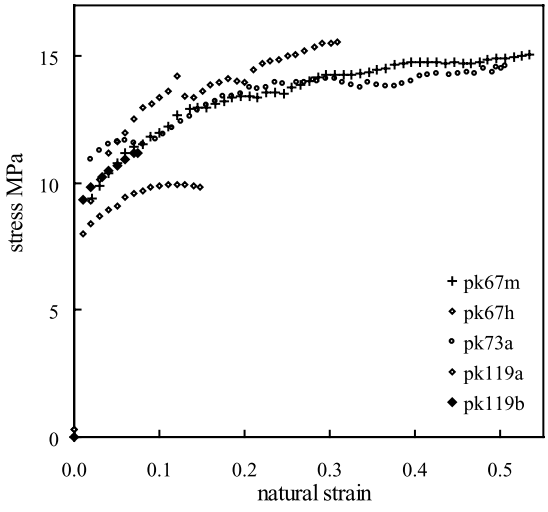

Fig. 1. Stress–strain curves for deformed NaCl (see Table 1, unsmoothed data, corrected for change in area and specimen length).

Table 1
Information on samples used in deformation experiments

Sample	Drying procedure	Water (ppm)	Grain size[a] (μm)	Natural strain
PK67	0.2 °C/min to 350 °C/16 h; 0.2 °C/min to 530 °C/68 h	–	310	Undeformed
PK67h	As for PK67	3		0.28
PK67m	As for PK67	6		0.54
PK73	1.5 °C/min to 560 °C/25 h	–	126	Undeformed
PK73a	As for PK73	7		0.5
PK119b	2 °C/min to 700 °C/1 h; 0.5 °C/min to 530 °C/44 h	7	329	0.07
PK119a	As for PK119a	11[b]	412	0.15

[a] Grain sizes of undeformed material were determined using linear intercept of at least 100 grains from light micrographs.
[b] Argon gas ran out during drying.

2.2. Microscopy and EBSD

The microstructures of deformed and undeformed material were examined using LM and orientation contrast in the scanning electron microscopy (SEM). Conditions used for EBSD mapping NaCl, 12 kV, 2 nA, were mostly the same as in previous work (Pennock et al., 2002; Pennock and Drury, 2005). EBSD data were collected and analysed using HKL Channel 5 software and either a Philips XL30 SEM with a SIT camera, or a Philips XL30 SFEG SEM and a Nordlys CCD camera.

In all EBSD work, a 4 μm step was used to determine misorientations of subgrains, which gave a reasonable representation of the subgrain microstructures (average subgrain size 12 μm) and misorientations; smaller step sizes required more time to comprehensively map grain misorientations and increased the relative number of non-indexed pixels along etched boundaries, whereas large step sizes cumulated orientations across several subgrains (Pennock et al., 2002). Smaller step sizes of 1–3 μm were used to examine details of subgrain microstructures.

The quality of the EBSD maps was good, as subgrain misorientations of 0.5° were resolved and showed good correlation with etched microstructures (Pennock and Drury, 2005). Maps were filtered to remove orientation noise using VMAP (in-house software, courtesy of F.J. Humphreys, Manchester University) (Humphreys et al., 2001). Filtering removed many of the low misorientations caused by orientation noise and poor pattern quality along boundaries. Filtering to remove low angle misorientations caused by noise allowed resolution of misorientations to better than 0.5° and gave a good representation of the etched microstructures. All EBSD maps are shown after filtering.

The frequency distribution of subgrain boundary length per unit area as a function of misorientation angle was determined from nearest neighbour pixel misorientations after replacing most non-indexed pixels with an average of nearest neighbour pixel orientations. The average misorientations of subgrains $>0.5°$ of individual grains were also calculated. At higher strains of about 0.5, a few subgrain boundaries completely enclosed regions to create new grains with grain boundary misorientations $>16°$. Distinguishing these boundaries from original grain boundaries was often not possible and these boundaries were not included in the average misorientation calculation. In many instances, segments of the subgrain boundary developed misorientations $>16°$, and these were included in the calculation of average misorientations, as the boundary segments did not completely surround a region to form a new grain. The arithmetic average of the grain average distributions, $\theta_{\text{av-grains}}$, was determined for each strain. Frequency distributions based on grain averages gave a good insight into the standard deviations and spread of average misorientations on a grain basis for a given strain. With knowledge of the standard errors, it was possible to assess the influence of grain size on average misorientation values.

3. Results

3.1. Microstructure

The undeformed material (Table 1) contained mostly polygonal recrystallized grains and the occasional square-shaped grain (Fig. 2a). One batch had a slightly lower original grain size of 126 ± 12 μm (PK73). A few grains contained subgrains with low misorientations, $<2°$, measured with EBSD. Sometimes larger grains contained remnant internal grains; the volume fraction of these grains was quite small, up to about 1% of the area in the 0.07 strained sample.

In the deformed samples grains became flattened with increasing strain and most grain boundaries remained smooth (Fig. 2b). Boundaries were preferentially etched and some porosity, mostly inter-granular, was observed, especially after cleaning samples with ether. There was evidence for a small amount of slow grain boundary migration in deformed samples in the form of micron-scale grain boundary serrations, which occurred at the intersection of subgrains with grain boundaries throughout materials with higher water contents (PK119a). All samples contained subgrains, although a few grains in each sample, usually with a grain size less than 100 μm, contained relatively few subgrains.

Qualitative assessment of the subgrain boundary

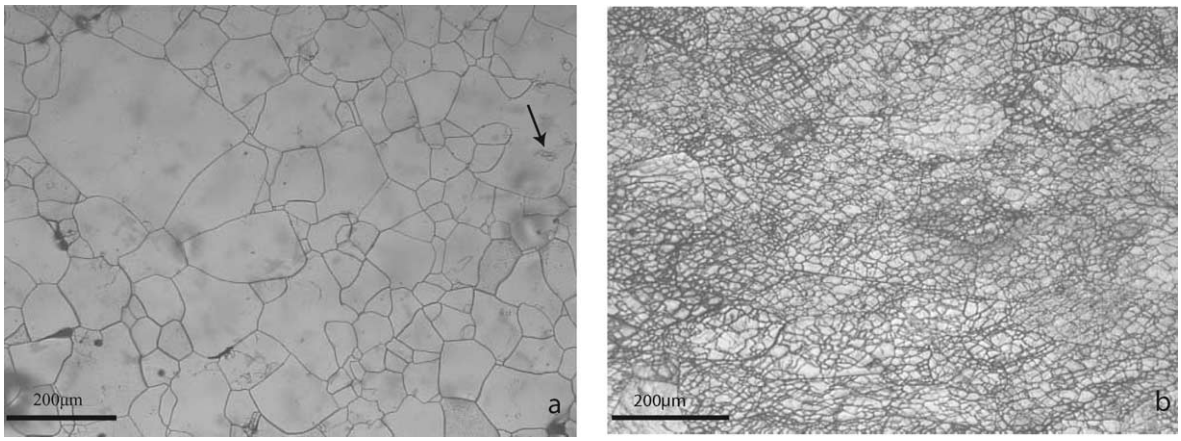

Fig. 2. Light micrographs showing typical grain shapes of: (a) undeformed (PK73) and (b) deformed material (PK73a). Arrow shows remnant, internal grains.

misorientations in EBSD mapped microstructures (Fig. 3 shows typical details as a function of strain) showed that there was considerable variation in the subgrain misorientations, both within individual grains and between grains. Individual segments of subgrain boundaries differed significantly in misorientation and it was unusual for an individual subgrain to be surrounded by misorientations $>5°$ at strains of 0.5. The micrographs show that equiaxed subgrains were ubiquitous at all strains and generally surrounded by boundaries with very low misorientations $<2°$; at strains of 0.28 and above a marked preferential alignment of these subgrain boundaries at about 45° to the compression axis was visible. In some grains extended subgrain boundaries (arrowed in Fig. 3) formed that were longer than the equiaxed subgrain size.

At the lowest strain, 0.07 (Fig. 3a), many of the subgrains were not completely enclosed by boundaries of $>0.5°$ misorientation, i.e. many subgrain boundaries had misorientations $<0.5°$. Extended subgrain boundaries developed at 0.07 strain with misorientations of 2–5° and some triple junctions showed extended subgrain boundaries with misorientations as high as 5–10°. A few grains (e.g. middle of lower grain, Fig. 3a) showed high misorientation boundaries in the central portion of the grain, which, by analogy with other microstructures, are thought to be associated with triple junctions of internal, or island, grains located beneath the mapped surface. At 0.15 strain (Fig. 3b) subgrains with boundary misorientations 0.5–2° were ubiquitous. These subgrain boundaries tended to surround equiaxed shaped subgrains. Extended subgrain boundaries showed an increase in misorientations to greater than 5°. At 0.28 strain, (Fig. 3c) the majority of subgrains were surrounded by boundaries with misorientations of at least 2–5°, and many extended subgrain boundaries reached 5–10°. At 0.5 strain (Fig. 3d) sections of extended boundaries had developed misorientations greater than 10° but the majority of equiaxed subgrain boundary misorientations remained less than 5°. These trends in subgrain boundary misorientations development with strain are shown in Fig. 4. The log–frequency distribution clearly shows that the majority of subgrain boundary misorientations have low misorientations $<5°$ even at strains of about 0.5.

Many extended subgrain boundaries were associated with triple junctions at all strains, others occurred in grains that split into widely differing orientations, often with a banded appearance. Grains, containing predominantly equiaxed or both equiaxed and extended subgrain boundaries, were selected (Table 2). The grains containing extended subgrain boundaries were generally oriented with ⟨110⟩ crystal axes at a high angle to the compression axis (see Table 2). As an individual grain orientation spread out with increasing strains, the original orientation was difficult to define. Extended subgrain boundaries did not generally surround individual subgrains, although corner sections of original grains were nearly 'cut-off' by high angle subgrain boundaries at higher strains. At higher strains, 0.5, some of the extended subgrain boundaries developed much smaller subgrains along their boundaries (Fig. 3d) many of which were smaller than the 4 μm step size used to map the average misorientations. Very occasionally, these small subgrains reached sufficient misorientation to form small new subgrains.

3.2. Average angular misorientations

The average misorientation values of selected grains after 0.54 strain (PK67m) are also shown in Table 2. Grains containing extended subgrain boundaries in addition to the equiaxed subgrain boundary types showed up to 1° variation in average misorientation and had higher average misorientations than grains in which extended subgrain boundaries were absent. The grains containing extended subgrain boundaries represented at least 37% of the mapped area.

Inverse pole figures (IPFs) for the compression axis obtained from EBSD maps of nearby locations in sample PK67m (0.54 strain) are shown in Fig. 5. Each map showed differences in texture and average misorientation values; in

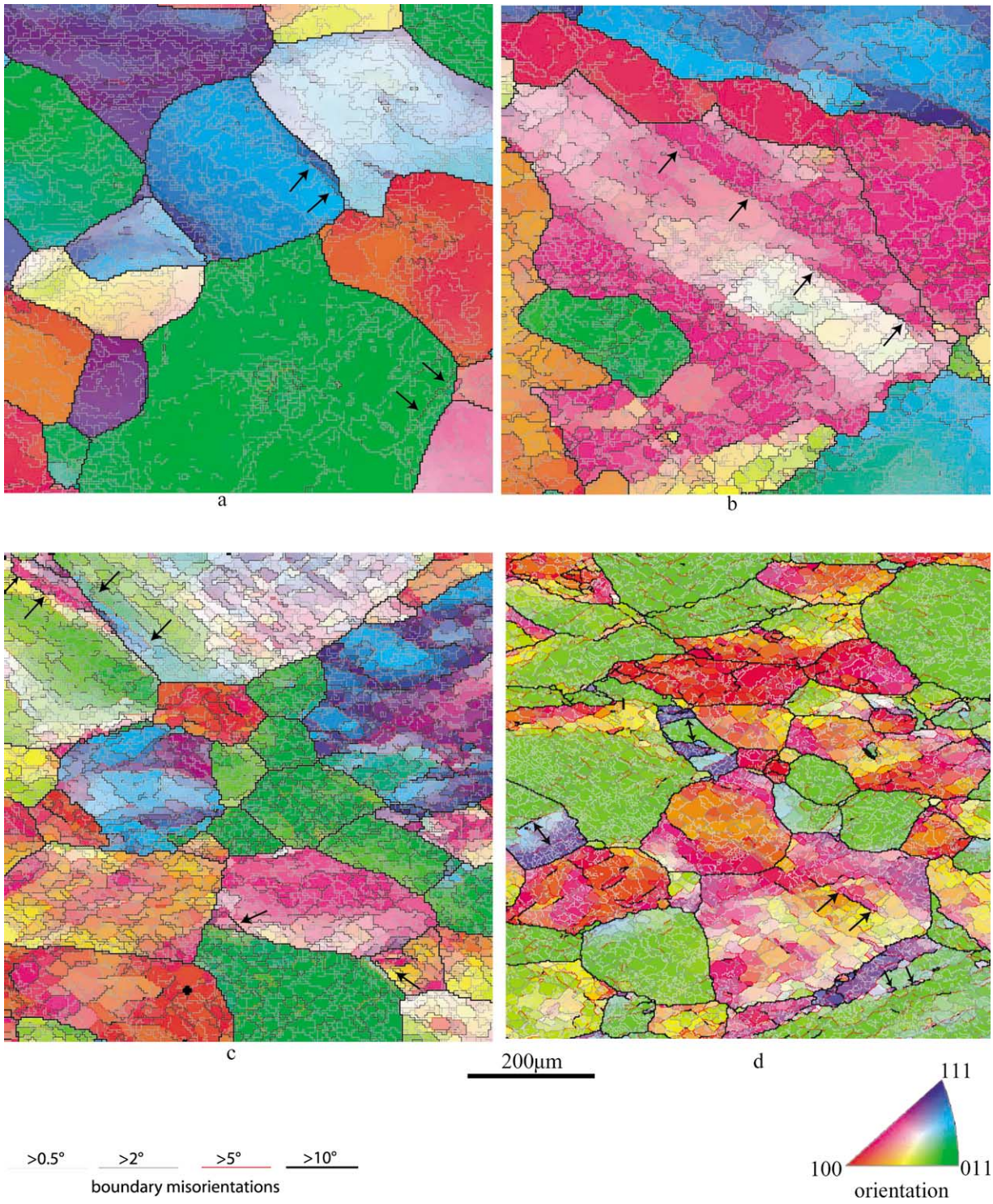

Fig. 3. EBSD micrographs of deformed material for strains: (a) 0.07, (b) 0.15, (c) 0.28 and (d) 0.5 (samples PK119b, 119a, 67h and 73a, respectively). Changes in orientation with respect to the compression axis (vertical) are shown in colour. Arrows show extended subgrain boundaries, which are often associated with high misorientations, as shown by change in colour within individual grains. In (d), smaller subgrains along extended subgrain boundaries are also arrowed. More subgrain detail is visible in (d) because the EBSD map was made with a 2 μm step size compared with a 4 μm step used in to (a)–(c).

general, a map with a single ⟨101⟩ fibre texture (Fig. 5c) had a lower average misorientation. The differences in average misorientation as a function of fibre texture subsets are given in Table 3 for two samples (PK73a and PK67m). In general, areas with ⟨111⟩, ⟨100⟩ and ⟨115⟩ fibres oriented approximately parallel to the compression axis had higher average misorientation than areas oriented with ⟨120⟩ or ⟨110⟩, although this trend was not so strong in sample

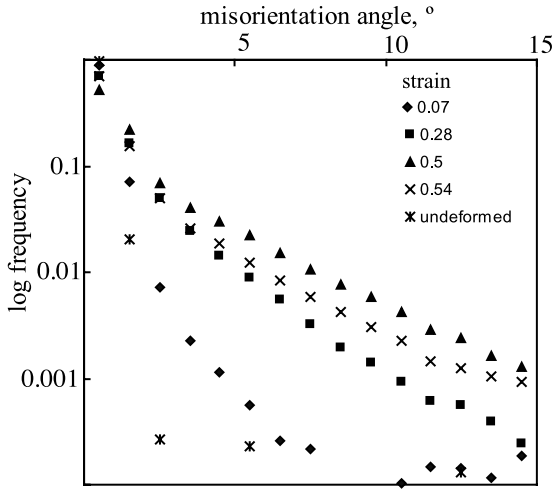

Fig. 4. Log–frequency distribution is shown for subgrain misorientations at different strains. Higher angle misorientations increase in frequency with strain, although the majority of misorientations remain less than 5°. Sample PK73a (strain 0.5) had a smaller initial grain size compared with other samples and shows a greater frequency of higher angle misorientations (SIT camera system, 4 μm step, unfiltered).

PK73a. Table 3 shows that the smaller grain size material (PK73a), 126 μm, had higher average misorientation values than the 310 μm (PK67m) grain size material deformed to approximately the same strain.

The frequency distribution of average misorientations of individual grains is shown in Fig. 6. As strain increased average misorientations of grains both increased and had a wider range of values. The average misorientations of these distributions, $\theta_{\text{av-grains}}$, which included all subgrain boundary misorientations $>0.5°$, are also given. These values are slightly larger at each strain than the θ_{av} values derived from misorientations in the range 0.5–16° (Pennock and Drury, 2005). Average misorientations based on grains, $\theta_{\text{av-grains}}$, are plotted for each strain in Fig. 7. Average misorientations increased with strain, although the rate of increase decreased at higher strains in samples with similar initial

Table 3
Average misorientations for different fibre textures in samples PK73a and PK67m. Fibre textures were made by selecting specific poles to be parallel, within 8° deviation, to the compression direction (4 μm step, unfiltered data, SIT camera system)

Fibre texture	Average misorientation ° (% data points)	
	Grain size 310 μm (PK67m)	Grain size 126 μm (PK73a)
111	1.70 (0.2)	1.72 (0.8)
100	1.50 (1.0)	1.83 (1.9)
115	1.56 (7.9)	1.81 (10)
120	1.33 (36.5)	1.75 (27.4)
110	1.37 (19.1)	1.73 (13.7)
Complete map	1.92	2.27

grain size. Average misorientations for samples of a similar grain size followed a power law relationship of the form:

$$\theta_{\text{av-grains}} = k_1 \varepsilon^n \quad (2)$$

where ε is the true strain, k_1 is a constant with a value of 3.3° and n, the power exponent, has a value of 0.42. Analysing the subgrain misorientation on a grain basis rather than on a map as a whole, and including all subgrain boundary misorientations, gives a slightly different result to earlier work in which EBSD maps as a whole were analysed in the angular range 0.5–16° (k_1 was found to have a value of 3.1° and n was 0.41) (Pennock and Drury, 2005). Therefore, it is important to use a similar analysis technique for etched NaCl when comparing data. Grain analysis is more time consuming, but is the better technique and provides information about errors and about the spread in orientation with strain of grains.

Sample PK73a, which had an original grain size of 126 μm and was strained to 0.5, showed a slightly higher average misorientation value compared with PK67m (original grain size 310 μm, strain 0.54). In order to determine whether this difference was significant, the average misorientation for PK67m was calculated for a strain of 0.5 using the appropriate values for the power law

Table 2
Average misorientations for selected grains and for the complete EBSD map (PK67m). The types of subgrain boundaries present and the approximate orientation of the grain with respect to the compression axis are given (0.54 strain, 4 μm step, unfiltered data, SIT camera system)

Subgrain boundary type	Average misorientation 0.5–<16°	Approximate orientation ⟨*uvw*⟩	% Data points
Complete map	1.92		100
Extended + equiaxed	1.74	115	3
	1.94	115	2
	2.64	115	1
	2.28	115	7
	1.83	115	3
	2.04	115	4
	1.76	441	1
	1.77	415	16
Equiaxed	1.42	110	5
	1.44	441	2
	1.35	Close 110	2
	1.34	Close 110	2
	1.34	Close 110	3

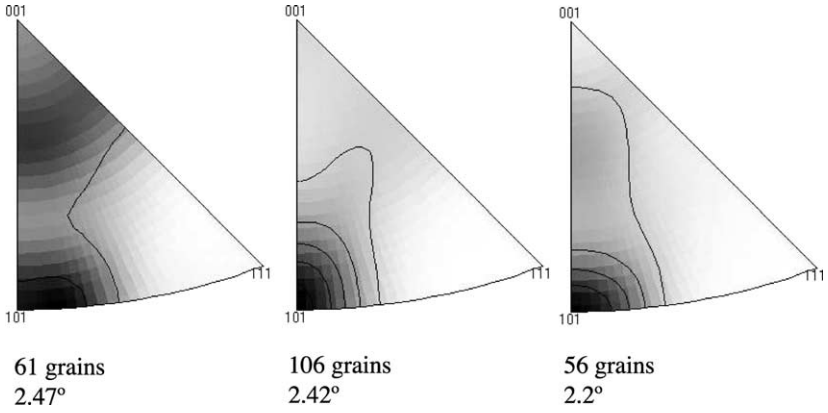

Fig. 5. Inverse pole figures for the compression axis direction, showing differences in texture between EBSD maps taken from nearby locations in the central portion of a deformed sample (PK67m). The number of grains mapped and the average misorientations for each map are also given. The strength of the ⟨101⟩ pole and the presence of other poles orientated away from ⟨101⟩ influence the average misorientation. Slightly lower misorientations are seen in maps with a single ⟨101⟩ maximum (contoured as multiples of uniform density, half width 10°, cluster size 5°).

relationship based on the grain averages ($n=0.42$ and $k_1=3.3°$) to give $2.46\pm0.11°$. This is slightly smaller than the value of $2.71\pm0.11°$ for PK73a (see Fig. 7).

4. Discussion

The main objectives of this work have been to examine the effect that strain, grain orientation, texture and grain size have on the average misorientation values in dry NaCl. The quality and processing of EBSD maps is briefly discussed, as these influence misorientation values. First, the microstructures are summarized.

As the presence of very small amounts of water assist rapid grain boundary migration (Watanabe and Peach, 2002) and removes subgrain misorientations (Trimby et al., 2000), the samples in this study were dried to very low water contents of a few ppm. The grain serrations and equant grains, which contained relatively few subgrains, suggest that a few regions underwent dynamic recrystallization by rapid grain boundary migration, probably assisted by localized pockets of water. However, the volume fraction of these grains was $<1\%$ and generally not included in EBSD maps used to calculate the average misorientations.

While samples were quenched from the deformation temperature at a practical rate, the cooling rates were relatively slow compared with rapid quenches used for unconfined deformation. Microstructures are therefore likely to have been fully recovered so that subgrain misorientations were probably slightly higher than at deformation temperatures. Nevertheless, misorientation–strain behaviour of NaCl shows a similar trend to that found

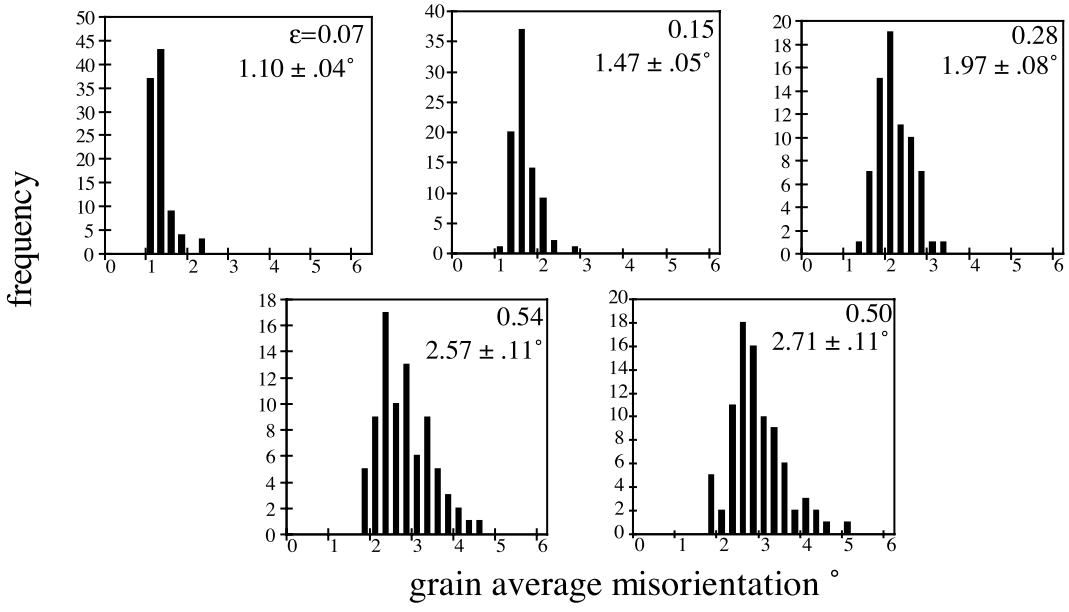

Fig. 6. Frequency distribution of grain average misorientations for different strains, ε. Averages of these distributions, $\theta_{\text{av-grains}}$, and standard errors at 90% confidence for about 80 grains, are shown.

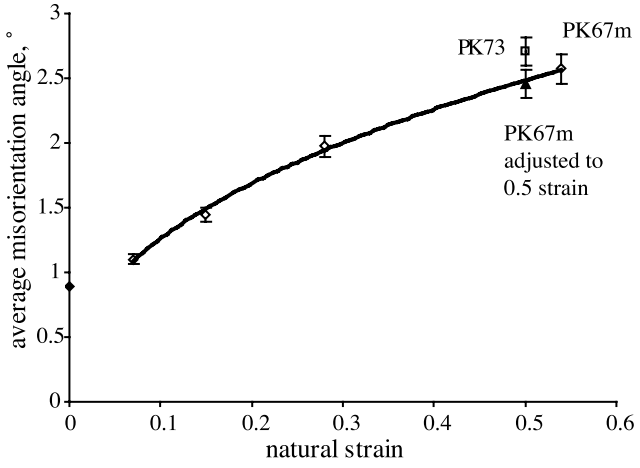

Fig. 7. Average misorientation of grain averages, $\theta_{av\text{-}grains}$, as a function of strain. Average misorientation increases with strain. A power law relationship trend line is shown, excluding sample PK73a, which had a smaller original grain sizes than other samples. The average misorientation value for sample PK67m is also shown adjusted to a strain of 0.5 (misorientation range $>0.5°$, CCD camera, at least 80 grains, 4 μm step maps).

for deformed metals (Hughes, 2002), which are generally rapidly cooled to retain the deformation microstructures. Furthermore, slower cooling rates are more likely to occur in naturally deformed rocks.

Deformation of dry NaCl at 0.4 Tm resulted in subgrain formation even at very low strains of 0.07. The types of subgrain boundaries present, equiaxed and extended, were similar to those reported for ⟨100⟩ single crystal experiments on NaCl (Raj and Pharr, 1989) and in cold (0.3 Tm) and hot (>0.5 Tm) worked aluminium and some aluminium alloys (Humphreys and Drury, 1986; Delannay et al., 2001; Barnett and Montheillet, 2002; Hurley and Humphreys, 2003).

As extended subgrain boundaries tended to form in grains that did not have ⟨110⟩ parallel to the compression axis, grain orientation is likely to be an important factor in determining the type of subgrain boundary and average misorientation of a grain. However, extended subgrain boundaries often formed across only part of a grain, implying that surrounding grain orientation also influenced the microstructure. This was most pronounced at triple junctions where the constraints of surrounding grains were the greatest.

With increasing strain, the different types of subgrain boundary in NaCl developed different ranges of misorientations (Fig. 3), with the result that by 0.54 strain average misorientations of individual grains typically differed by about 1° (Table 2), but differences could reach 3° (Fig. 6). These misorientation differences are likely to have a considerable effect on the stored energy of different grains, with important implications for recrystallization. As 500–1000 grains are needed to describe fully bulk textures, variations in texture occur between individual EBSD maps containing relatively few grains. Variations in texture can cause differences in average misorientation between samples or sub-areas and are likely to cause the spread in average misorientation values observed for EBSD maps from areas containing only 10s of grains (Fig. 5 and Table 2). Misorientations from at least 80 grains are needed to determine a representative average misorientation value for a particular material state of strain or recrystallization. Furthermore, the step size used to map subgrain microstructures should be small enough so that individual subgrain boundaries are measured (Pennock et al., 2002). Obtaining accurate values of the average misorientation is therefore demanding on EBSD mapping times, particularly for larger grain size materials requiring small step mapping. Further work is needed on duplicate samples to assess the sample to sample variation.

EBSD mapping of etched NaCl contains more artefact misorientations along boundaries than found in other materials, because of the etch topography. The EBSD camera system used to map misorientations was found to affect average misorientation values and filtering maps increased misorientations (Pennock and Drury, 2005). These differences were explained in terms of the percentage of non-indexed pixels present in the maps and were not so pronounced in other materials in which subgrain boundaries were not etched (Hurley and Humphreys, 2002). An improved polishing method for NaCl should improve the map quality and reduce the differences in average misorientation values caused by noise reduction and filtering to reduce noise.

In material deformed to strains of at least 0.15, many subgrain misorientations were above the angular resolution limit of 0.5° and average misorientation values based on misorientations $>0.5°$ were representative. However, after very low strain deformation (<0.07) proportionally more misorientations were present that were below the angular resolution limit for EBSD. Average misorientation values at low strains were therefore slightly overestimated. For similar reasons, the average misorientation of the undeformed material was far higher than expected (Fig. 7). For this reason, the trend lines used to fit the $\theta_{av\text{-}grains}$ versus ε data were calculated using the data for the 0.07–0.54 strained samples and the undeformed average misorientation value was rejected. The expected trend would be for the undeformed average misorientation to go through zero and a power law relationship satisfies this constraint.

Providing the EBSD data collection and processing are similar, the average misorientations can be fitted to a power law relationship given by Eq. (2), with coefficients of determination, R^2, better than 0.99 and $n \sim 0.4$ (Pennock and Drury, 2005). This is an encouraging result and suggests that an average misorientation–strain relationship determined using EBSD might provide useful information about strain accommodated by dislocation creep in a material.

Our data on samples PK73a and PK67m (Figs. 6 and 7) suggest that the average subgrain misorientation in dry NaCl

may be slightly dependent on the initial grain size, such that a higher misorientation occurs in a smaller grain size material. Theoretical models for polycrystalline plasticity (Ashby, 1970) imply that the grain size will influence the accommodation strains required to maintain compatibility between different grains. In Ashby's model the misfit is accommodated by a density, ρ_g, of homogeneously distributed geometrically necessary dislocations:

$$\rho_g = \bar{e}/4bD \tag{3}$$

where $\bar{e}$ is the average strain, b the Burgers vector and D the grain size. If the dislocations are arranged by recovery into subgrain walls, with an average misorientation, θ_g, across the walls, ρ_g can be expressed in terms of θ_g (Hughes et al., 2003):

$$\rho_g = S_v\theta_g/b \tag{4}$$

where S_v is the boundary area per unit volume, which is equal to $2/L$ (Pickering, 1976): setting L, the mean intercept length to d_g, the average spacing for geometric subgrain boundaries, gives:

$$\theta_g = k_2\bar{e}d_g/D \tag{5}$$

where k_2 is a constant. Thus at constant subgrain size, i.e. constant stress, the average misorientation for geometric subgrain boundaries is a function of average strain, grain size and average spacing for geometric subgrain boundaries.

Subgrains may also form by statistical (or incidental) trapping of dislocations into boundaries (Kuhlmann-Wilsdorf and Hansen, 1991), with an average spacing d_s, and theoretical studies (Pantleon, 1998) suggest that θ_s, the average misorientation across statistical subgrain boundaries is independent of grain size for a constant subgrain size:

$$\theta_s = k_3\sqrt{(\bar{e}/d_s)} \tag{6}$$

where k_3 is a constant.

Geometrical and statistical subgrain boundary misorientations have been studied using TEM (Hughes et al., 1997, 2003). Hurley and Humphreys (2003) argue that their equiaxed subgrains identified with EBSD are likely to be statistical in origin and the extended subgrain boundaries observed in the current work in NaCl are probably geometric in origin.

The microstructures shown in Fig. 3, showing extended subgrain boundaries dissecting grains and emanating from triple junctions, suggest that the spacing of geometric subgrain boundaries, d_g, depend on grain size, D. These subgrain types have a much larger spacing than equiaxed subgrains and in the limit when a grain splits itself into two subgrains, can approach the grain size. If d_g can be expressed as some factor of grain size, D/x, where in the most simple form x is a constant, then Eq. (5) for geometric average misorientations becomes dependent only on strain:

$$\theta_g \propto \bar{e} \tag{7}$$

A similar result can be derived for core–mantle microstructures, in which a mantle of higher misorientation subgrain boundaries occurs: the grain size, D, in Eq. (5), can be replaced by a mantle width, which can be expressed in terms of some multiple of the subgrain size, d_g. Statistical subgrains are not expected to depend on grain size.

An estimation of the grain size effect for geometric subgrains can be made from the gradient of a log θ_g versus log D plot (Eq. (5)), which gives a slope of -1 for the Ashby model. In our work, in which the subgrain size is approximately constant, and no distinction was made between d_g and d_s, a slope of -0.1 was found (for PK73a and PK67m, average misorientations and grain sizes are, respectively, 2.71 and 2.46° and 126 and 310 μm). The grain size effect on average misorientations found for NaCl is therefore much weaker than that predicted by Ashby's model (Eq. (5)) and consistent either with Eq. (7) for geometric subgrains, or a dominance of statistical subgrain boundaries (Eq. (6)).

Most studies, however, predict that subgrain size, d, is dependent on stress, σ, with:

$$d \propto 1/\sigma^p \tag{8}$$

where p is a constant (Raj and Pharr, 1989; Hampel et al., 1998; Stone et al., 2004); for NaCl single crystals, p was found to have a value of 1.1 for extended subgrain boundaries and 0.45 for equiaxed subgrains (Raj and Pharr, 1989). If d_g is solely dependent on stress, substituting in Eq. (5) gives a relationship in which θ_g is dependent on strain, grain size and stress:

$$\theta_g \propto \bar{e}/(\sigma^{1.1}D) \tag{9}$$

Similarly, substituting for statistical subgrains, d_s, in Eq. (6) gives:

$$\theta_s \propto \sqrt{(\bar{e}\sigma^{0.45})} \tag{10}$$

i.e. statistical subgrain boundary misorientations depend on strain and stress. However, the stress dependence for θ_s is in the opposite sense to that given for θ_g. The average misorientation of a microstructure will therefore depend on the balance of statistical and geometric subgrain boundary types. In the present study, samples work hardened, and subgrain misorientations may have been influenced by both stress and strain. Further work is needed to determine whether a power law relationship holds under steady state conditions.

The EBSD determined strain exponent value, n, for NaCl, 0.42, is lower than predicted in Eq. (5) for geometric boundaries, where n is 1, and approaches that predicted in Eq. (6) for statistical subgrain boundaries, where n is 0.5. However, Ashby's model does not take into account texture development, or multiple slip, and these effects are expected to reduce the strain dependence of θ_g at higher strain (Leffers, 1975). Other theoretical studies, based on finite

element modelling of fcc systems, also predict a power law relationship between the average misorientation and strain, with n, the strain exponent equal to 0.5 for θ_s and 0.7 for θ_g (Mika and Dawson, 1998), in agreement with Pantleon's model, Eq. (6) (Pantleon, 1998). A value of $n=0.68$ can also be determined from Leffers' model (Leffers, 1975) for geometric dislocations. The theoretical model agrees with the experimental TEM studies on fcc metals deformed over a wide range of temperatures (Hughes et al., 1997, 2003; Hughes, 2002). The lower values for NaCl might be caused by an overestimate of the low strain misorientation value, as discussed earlier, or by a difference in crystalline plasticity between NaCl and metals, or by a difference in the deformation mode, as the current work was based on compressive deformation and other experimental and theoretical studies were based on rolled deformation microstructures, which develop different textures.

A further consideration to the application of average misorientation value to determine strain is the effect of texture on the average misorientation values. The current work is based on samples with an almost random initial texture (Pennock et al., 2004). Final textures depend on the strain path and might influence misorientation values. As misorientations vary with texture and grain orientation, the average misorientation values in a rock with an initial texture is likely to develop different average misorientation values. An orientation dependence could also result in different average misorientation–strain relationships for compression, pure shear, tension and torsion deformation paths, depending on the texture differences that develop.

A potential application of the average misorientation strain relationship would be to estimate the strain produced by dislocation creep in naturally and experimentally deformed rocks. If dislocation creep is the sole mechanism then the average subgrain misorientation could be used to estimate finite strain in naturally deformed rocks. The average misorientation versus strain relationships may need to be calibrated for the effects of initial grain size and stress. Inherited microstructures from earlier deformation events will limit the applicability of the average misorientation–strain relationship; for example undeformed sediments may contain many grains with inherited subgrains.

In addition, average subgrain misorientations will only provide an estimate of the dislocation creep strain if static and dynamic grain boundary migration is limited. As extensive migration consumes old grains and subgrain boundaries, average misorientations depend only on the strain increment since the crystal was swept by a high-angle grain boundary. For example, in quartz average strain estimates based on subgrain misorientations will be applicable in the recovery controlled creep regime (Hirth and Tullis, 1992; Tullis, 2002), which is common during deformation at greenschist facies conditions (Stipp et al., 2002). At higher temperatures in quartz extensive grain boundary migration often occurs (Stipp et al., 2002). In naturally deformed NaCl the presence of grain boundary fluids results in extensive grain boundary migration during plastic deformation at low temperatures (Urai et al., 1987). Thus, average misorientations in highly deformed natural NaCl will only reflect the local post-recrystallization dislocation creep strain. If strains are too low for the onset of extensive grain boundary migration (Watanabe and Peach, 2002) then average misorientations in natural NaCl may be used to estimate strains produced by dislocation creep. The application of average misorientations to estimate strain will clearly be limited by static recrystallization, which will remove subgrains. Static recovery may also alter average misorientations.

As discussed above, the average misorientation of undeformed or very low strained material is overestimated. As grain boundary migration recrystallization also creates an inhomogeneous distribution of subgrains, from fully recrystallized grains to heavily deformed grains, an overestimation of average misorientations values is also expected for these microstructures. An alternative approach for determining strain from subgrain misorientation measurements is therefore needed for microstructures that are recrystallized by grain boundary migration, or for very low strained material in which the majority of the subgrain misorientations are below the angular resolution limit for EBSD. An alternative method for determining an average misorientation–strain relationship for these microstructures would be to include all mapped misorientations, not just a selected angular range, and to scale the average misorientation values in terms of mapped area, to give a boundary density (Wheeler et al., 2003). Another approach to assessing strain, which might be more applicable to naturally deformed rocks in which subgrain microstructures have low misorientations or are inhomogeneously distributed, might be to examine misorientation gradients within individual grains (Barton and Dawson, 2001; Pennock et al., 2002; Kamaya et al., 2005).

Microstructural studies show clear evidence for the operation of multiple deformation mechanisms in naturally deformed rocks (Mitra, 1976; White, 1982; Knipe, 1989; Stöckhert et al., 1999; Harrison and Onasch, 2000). If microstructures are grouped by deformation mechanism then crystal plastic microstructures are often the most pervasive in naturally deformed quartz rocks (Harrison and Onasch, 2000; Tullis, 2002). However, pervasive undulatory extinction, deformation bands and subgrains may be produced by relatively low strains so quantitative methods are needed to determine how strain is partitioned between different mechanisms (Mitra, 1976; Onasch et al., 1997). The strain produced by dislocation creep can be estimated from lattice rotations in deformation bands (Wu and Groshong, 1991) and from deformed rutile needles in quartz grains (Mitra, 1976). With suitable experimental calibrations, for subgrain size with stress, and for grain size, average subgrain misorientations measured by EBSD might be used to estimate dislocation creep strains.

The average misorientation determined using EBSD is a

useful measure of strain involving dislocation creep for experimentally deformed materials and might be very useful in assessing strain partitioning, providing EBSD mapping data are collected with a suitable step size and processed in a similar manner. However, there are practical limitations to applying this technique to naturally deformed rocks, such as mapping large grain sizes with a small step size, or mapping microstructures where the subgrains are inhomogeneously distributed. Furthermore, in theory, the misorientation–strain relationship is stress dependent and needs to be calibrated to account for differences caused by textures and grain sizes.

5. Conclusions

1. In dry, synthetic NaCl, the average misorientation of subgrains measured using EBSD can be expressed as a function of strain in terms of a power law relation, of the form $\theta_{\text{av-grains}} = k_1 \varepsilon^n$, with n approximately equal to 0.4. This relationship holds for a material of constant grain size deformed in compression, providing EBSD processing is similar.
2. The average misorientation shows a weak grain size dependence, with higher misorientations occurring in smaller grain sized material. This is also consistent with some models of polycrystalline plasticity.
3. Current theory for subgrains suggests that average misorientations may also be stress dependent.
4. Subgrain misorientations are influenced strongly by grain orientation and surrounding grains and hence the average misorientation–strain relationship may be texture dependent.
5. Measurement of at least 80 grains is needed for an accuracy of 0.11° in the average misorientation.
6. It may be possible to use average misorientation values to estimate strain contribution by dislocation creep in rock materials, notably NaCl.

Acknowledgements

Peter van Krieken is thanked for carrying out the deformation experiments and Jaap Liezenberg for sample preparation. We thank Michael Stipp and an anonymous reviewer for constructive criticism that helped to improve this manuscript. The electron microscopy was conducted at the Electron Microscopy and Structure and Analysis centre at Utrecht University.

References

Ashby, M.F., 1970. The deformation of plastically non-homogeneous materials. Philosophical Magazine 21, 399–424.

Avé Lallement, H., 1985. Subgrain rotation and dynamic recrystallization of olivine, upper mantle diaperism, and extension of the basin-and-range province. Tectonophysics 119, 89–117.

Barnett, M.R., Montheillet, F., 2002. The generation of new high-angle boundaries in aluminium during torsion. Acta Materiala 50, 2285–2296.

Barton, N.R., Dawson, P.R., 2001. A methodology for determining average lattice orientation and its application to the characterization of grain substructure. Metallurgical and Materials Transactions A 32A, 1967–1975.

Carter, N.L., Heard, H.C., 1970. Temperature and rate dependent deformation of halite. American Journal of Science 269, 193–249.

Delannay, L., Mishin, O.V., Jensen, D.J., Van Houtte, P., 2001. Quantitative analysis of grain subdivision in cold rolled aluminium. Acta Materialia 49 (13), 2441–2451.

Hampel, A., Hunshce, U., Weidinger, P., Blum, W., 1998. Description of the creep of rock salt with the composition model—II. Steady-state creep. In: Aubertin, M., Hardy Jr., H.R. (Eds.), The Mechanical Behaviour of Salt Proceedings of the Fourth Conference. Trans. Tech. Publications, pp. 287–299.

Harrison, M.J., Onasch, C.M., 2000. Quantitative assessment of low temperature deformation mechanisms in a folded quartz arenite, Valley and Ridge Province, West Virginia. Tectonophysics 317, 73–91.

Hirth, G., Tullis, J., 1992. Dislocation creep regimes in quartz aggregates. Journal of Structural Geology 14, 145–159.

Hughes, D.A., 2002. Scaling of deformation-induced microstructures in fcc metals. Scripta Materialia 47, 697–703.

Hughes, D.A., Liu, Q., Chrzan, D.C., Hansen, N., 1997. Scaling of microstructural parameters: misorientations of deformation induced boundaries. Acta Materialia 45 (1), 105–112.

Hughes, D.A., Hansen, N., Bammann, D.J., 2003. Geometrically necessary boundaries, incidental dislocation boundaries and geometrically necessary dislocations. Scripta Materialia 48, 147–153.

Humphreys, F.J., 2001. Review: grain and sub-grain characterization by electron backscatter diffraction. Journal of Materials Science 36, 3833–3854.

Humphreys, F.J., Drury, M.R., 1986. The formation of high angle grain boundaries and new grains during the deformation of Al–5%Mg at elevated temperatures. In: Aluminium Technology 3. Institute of Metals, London, pp. 76.1–76.5.

Humphreys, F.J., Bate, P.S., Hurley, P.J., 2001. Orientation averaging of electron backscattered diffraction data. Journal of Microscopy 201 (1), 50–58.

Hurley, P.J., Humphreys, F., 2002. Characterizing the deformed state in Al–0.1 Mg alloy using high-resolution electron backscattered diffraction. Journal of Microscopy 205 (3), 218–225.

Hurley, P.J., Humphreys, F.J., 2003. The application of EBSD to the study of substructural development in a cold rolled single-phase aluminium alloy. Acta Materialia 51 (4), 1087–1102.

Kamaya, M., Wilkinson, A.J., Titchmarsh, J.M., 2005. Measurement of plastic strain of polycrystalline material by electron backscattered diffraction. Nuclear Engineering and Design 235 (6), 713–725.

Knipe, R.J., 1989. Deformation mechanisms—recognition from natural tectonites. Journal of Structural Geology 11, 127–146.

Kuhlmann-Wilsdorf, D., Hansen, N., 1991. Geometrically necessary, incidental and subgrain boundaries. Scripta Metallurgica et Materialia 25 (7), 1557–1562.

Leffers, T., 1975. On the misfit between grains in a deformed Sachs polycrystal and its relation to the homogeneous deformation of real polycrystals. Scripta Metallurgica 9, 261–264.

Mika, D.P., Dawson, P.R., 1998. Polycrystal plasticity modeling of intracrystalline boundary textures. Acta Materialia 47 (4), 1355–1369.

Mitra, S., 1976. A quantitative study of deformation mechanisms and finite strains in quartzites. Contributions to Mineralogy and Petrology 59, 203–226.

Onasch, C.M., Shen-Tu, B., Couzens-Schultz, B.A., 1997. Strain partitioning and factorization in a quartz arenite. Journal of Structural Geology 20, 1065–1074.

Pantleon, W., 1998. On the statistical origin of disorientations in dislocation structures. Acta Materiala 46 (2), 451–456.

Passchier, C.W., Trouw, R.A.J., 1996. Microtectonics. Springer, Berlin.

Peach, C.J., Spiers, C.J., 1996. Influence of crystal plastic deformation on dilatancy and permeability development in synthetic salt rock. Tectonophysics 256 (1–4), 101–128.

Pennock, G.M., Drury, M.R., 2005. Low angle subgrain misorientations in deformed NaCl. Journal of Microscopy 217, 130–137.

Pennock, G.M., Drury, M.R., Trimby, P.W., Spiers, C.J., 2002. Misorientation distributions in hot deformed NaCl using electron backscattered diffraction. Journal of Microscopy 205 (3), 285–294.

Pennock, G.M., Drury, M.R., Spiers, C.J., 2004. Investigation of subgrain rotation recrystallization in dry polycrystalline NaCl. Materials Science Forum 467–470, 597–602.

Pickering, F.B., 1976. The Basis of Quantitative Metallography. Institute of Metallurgical Technicians, pp. 1–38.

Raj, S.V., Pharr, G.M., 1989. Creep substructure formation in sodium chloride single crystals in the power law and exponential creep regimes. Materials Science and Engineering, A A122, 233–242.

Randle, V., Engler, O., 2000. Introduction to Texture Analysis: Macrotexture, Microtexture and Orientation Mapping. Gorden & Breach Science Publications.

Spiers, C.J., Carter, N.L., 1998. Microsphysics of rocksalt flow in nature. In: Aubertin, M., Hardy Jr., H.R. (Eds.), The Mechanical Behaviour of Salt IV—Proceedings of the Fourth Conference Series on Rock and Soil Mechanics. Trans. Tech. Publications, pp. 115–128.

Spiers, C.J., Urai, J.L., Lister, G.S., Boland, J.N., Zwart, H.J., 1986. The Influence of Rock–Fluid Interaction on the Rheological and Transport Properties of Dry and Wet Salt Rocks, European Communities Commission, Nuclear Science and Technology Series 1986.

Spiers, C.J., Schutjens, P.M.T.M., Brzesowsky, R.H., Peach, C.J., Liezenberg, J.L., Zwart, H.J., 1990. Experimental determination of constitutive parameters governing creep of rocksalt by pressure solution. In: Knipe, R.J., Rutter, E.H. (Eds.), Deformation Mechanisms, Rheology and Tectonics. The Geology Society, London, Special Publication 54, 215–227.

Stipp, M., Stunitz, H., Heilbronner, R., Schmid, S.M., 2002. Dynamic recrystallization of quartz: correlation between natural and experimental conditions. In: De Meer, S., Drury, M.R., De Bresser, J.H.P., Pennock, G.M., (Eds.), The Geological Society, London, Special Publication, 200, 171–190.

Stöckhert, B., Brix, M.R., Kleinschrodt, R., Hurford, A.J., Wirth, R., 1999. Thermochronometry and microstructures of quartz—a comparison with experimental flow laws and predictions on the temperature of the brittle–plastic transition. Journal of Structural Geology 21 (3), 351.

Stone, D.S., Plookphol, T., Cooper, R.F., 2004. Similarity and scaling in creep and load relaxation of single-crystal halite, (NaCl). Journal of Geophysical Research 109 (B12), B12201.

Ter Heege, J.H., 2002. Relationship between dynamic recrystallization, grain size distribution and rheology. PhD Thesis, Utrecht University.

Ter Heege, J., De Bresser, J.H.P., Spiers, C.J., 2005. Dynamic recrystallization of wet synthetic polycrystalline halite: dependence of grain size distribution on flow stress, temperature and strain. Tectonophysics 396, 35–57.

Trimby, P.W., Drury, M.R., Spiers, C.J., 2000. Recognising the crystallographic signature of recrystallization processes in deformed rocks: a study of experimentally deformed rocksalt. Journal of Structural Geology 22 (11–12), 1609–1620.

Tullis, J., 2002. Deformation of granitic rocks: experimental studies and natural examples. In: Karato, S., Wenk, H.-R. (Eds.), Plastic Deformation of Minerals and Rocks. Reviews in Mineralogy and Geochemistry, vol. 51. Mineralogical Society of America, pp. 51–95.

Urai, J.L., Spiers, C.J., Zwart, H.J., Lister, G.S., 1986. Weakening of rock salt by water during long-term creep. Nature 324, 554–557.

Urai, J.L., Spiers, C.J., Peach, C.J., Franssen, R.C.M.W., Liezenberg, J.L., 1987. Deformation mechanisms operating in naturally deformed halite rocks as deduced from microstructural investigations. Geologie en Mijnbouw 66, 165–176.

Watanabe, T., Peach, C.J., 2002. Electrical impedance measurement of plastically deforming halite rocks at 125 °C and 50 MPa. Journal of Geophysical Research 107(B1), ECV 2, 1–12.

Wheeler, J., Jiang, Z., Prior, D.J., Tullis, J., Drury, M.R., Trimby, P.W., 2003. From geometry to dynamics of microstructure: using boundary lengths to quantify boundary misorientations and anisotropy. Tectonophysics 376, 19–35.

White, J.C., 1982. Quartz deformation and the recognition of recrystallization regimes in the Flinton Group conglomerates, Ontario. Canadian Journal of Earth Sciences 19, 81–93.

Wu, S., Groshong, R.H., 1991. Strain analysis using quartz deformation bands. Tectonophysics 190, 269–282.